JOURNAL OF CATALYSIS 116, 383–398 (1989)

Importance of the Anatase–Rutile Phase Transition and Titania Grain Enlargement in the Strong Metal–Support Interaction Phenomenon in Fe/TiO_2 Catalysts

A. NOBILE, JR.,[1] AND M. W. DAVIS, JR.

Department of Chemical Engineering, University of South Carolina, Columbia, South Carolina 29225

Received August 18, 1988; revised November 7, 1988

The strong metal–support interaction (SMSI) in the system consisting of iron supported on high-surface-area titania powder was investigated. By observation of the anatase–rutile phase transition, titania grain enlargement, and the SMSI effect at several reduction temperatures in the range 643–873 K, it was found that these three phenomena occur simultaneously at reduction temperatures above 723 K. This suggests that the three phenomena are interrelated, and that the phase transition and grain enlargement are important factors concerning SMSI in high-surface-area powder samples. A mechanism has been proposed whereby Ti^{3+} defect centers in the titania lattice formed from support reduction are responsible for acceleration of phase transition and grain enlargement, and the TiO_x species that migrates onto supported metal particles is formed during the chaotic state of simultaneous phase transition and grain enlargement. At the temperature of the onset of the above three phenomena (~723 K), a stabilization against high-temperature sintering of iron particles became evident, suggesting that this effect becomes operative at the onset of SMSI. Iron particles supported on rutile were significantly smaller than anatase-supported particles which were reduced at the same temperature. The rutile was formed from anatase before impregnation with iron by reduction in hydrogen at 873 K followed by oxidation with oxygen at 473 K. The smaller iron particles and incomplete iron reduction were attributed to O_2^- ions adsorbed to the titania surface which acted to anchor Fe^{3+} and/or Fe^{2+} ions to the support, preventing their migration and combination to form large fully reduced iron particles.

INTRODUCTION

In 1978 it was reported that the chemisorption capacities of group VIII noble metals supported on titania were drastically suppressed due to a strong metal–support interaction (SMSI) after hydrogen reduction at temperatures near 773 K (*1*). The anomalous chemisorption behavior was attributed to chemical interaction between metal and support, such as bonding of noble metal atoms to surface titanium ions, or intermetallic compound formation. Similar decreases in chemisorption capacities after reduction at high temperatures were later noted with iridium supported on a series of other oxides (*2*). In fact, it was observed that the extent of chemisorption suppression correlated well with the reducibility of the support. Increased *d*-orbital occupancy of the support, with subsequent covalent bond formation between support metal ions and supported metal atoms, was proposed as a possible mechanism for the effect. Theoretical calculations performed by Horsley (*3*) on surface clusters formed between Pt and the $(TiO_6)^{8-}$ octahedron indicated that indeed covalent sharing between Pt and the support surface is likely if one of the oxygen atoms is removed from the octahedron. It has been established that titania is reduced in hydrogen at temperatures where SMSI is observed (*4–7*). Ultraviolet and x-ray photoelectron spectroscopic measurements have indicated reductions in binding energies of titania-supported metals, pro-

[1] Present address: E. I. du Pont de Nemours and Company, Inc., Savannah River Laboratory, Aiken, SC 29808.

0021-9517/89 $3.00

viding evidence for increased electron density of the metal (*8–10*). Thus, reduction of the support and subsequent electronic interaction with supported crystallites seemed plausible. Several other studies proposed similar electronic interactions between metal and support as the origin of SMSI (*11–13*).

Evidence suggestive of a different mechanism for the metal–support interaction in metal–titania systems was provided in a study by Simoens *et al.* (*14*), who prepared a special model catalyst by evaporating a nickel film onto a surface having areas of silica and titania. After reduction, Auger analysis detected titanium, nickel, and oxygen on the nickel covering the titania surface, whereas only nickel was detected on the regions overlaying silica. This result suggested that a titania species had migrated onto the nickel surface. Similar observations were made by Sadeghi and Henrich (*15*) with a model catalyst consisting of rhodium evaporated onto a titania single crystal. After H_2 or vacuum reduction at 673 K, they obtained surface depth profiles by monitoring Auger signals while sputtering with Ar^+ ions. The initially high oxygen and titanium signals, which sharply decreased as the rhodium signal increased, suggested that a titanium species had migrated onto the rhodium surface. This was supported by the observation that before sputtering the surface would not chemisorb CO, but after sputtering CO chemisorption occurred. Other studies provided evidence that the surface properties of titania-supported crystallites were influenced by diffusion of titania adspecies to particle surfaces (*16–19*).

Recently, Raupp and Dumesic (*20*) have demonstrated the presence of both diffusional and electronic effects in a model Ni/TiO_2 catalyst. Nevertheless, when metal–titania catalysts are reduced at temperatures in excess of 773 K, several phenomena are known to occur. Reduction of the support has been reported at temperatures below 773 K (*4–7*). The anatase–rutile phase transition has been observed at temperatures as low as 623 K for samples treated in hydrogen (*21–23*). Loss in support surface area has also been observed at 673 K and higher (*24, 25*); and the well-known metal–support interaction becomes evident at temperatures near 773 K and higher. Thus, it appears that with high-surface-area titania-supported metals, the anatase–rutile phase transition and surface area loss may be occurring in samples reduced near 773 K where the SMSI effect is observed. It is therefore important to determine what effect, if any, these phenomena have on the metal–support interaction. In this investigation, the properties of titania-supported iron crystallites, as well as the phase composition and morphology of the support, were studied over a range of reduction temperatures which included the temperature at which SMSI occurs. It was noted that the anatase–rutile phase transition, growth of titania grains, and the SMSI effect all occurred simultaneously at reduction temperatures above 723 K. This suggests that these three phenomena are interrelated, and that the phase transition and grain growth are important phenomena concerning SMSI. A mechanism is proposed which takes into account these and other observations.

EXPERIMENTAL

Catalyst preparation. All catalysts were prepared using Degussa P-25 TiO_2. x-Ray diffraction analysis of the material indicated that it was approximately 15% rutile, 85% anatase. No other phases could be detected in the diffraction patterns. Catalyst samples were prepared by incipient wetness impregnation with saturated solutions of $Fe(NO_3)_3 \cdot 9H_2O$ (99.997%, Aldrich) in 1 and 2 *M* HNO_3 and in dimethyl formamide (DMF). This was done to determine the effect of acid concentration on the resulting catalyst, as well as to determine if any differences exist between catalysts prepared with aqueous and organic impregnating solvents. The nitric acid and DMF used were

both reagent grade, and were obtained from Fisher Scientific. Impregnation was accomplished by dropwise addition of 0.25 ml of solution per gram of titania powder, after which samples were air-dried at 393 K for 24 h. Two successive impregnations in this manner yielded samples with composition between 6 and 7 wt% iron. The exact composition was determined by inductively coupled plasma (ICP) spectroscopic analysis of solutions obtained by dissolution of catalyst samples in an HF/H_2SO_4 mixture.

Samples (0.95 g) were placed in a quartz adsorption cell, and were reduced in flowing hydrogen (1.7 ml s^{-1}). The hydrogen (99.995%, Airco) was purified by passage through an Engelhard Deoxo purifier, followed by passage through a molecular sieve trap immersed in liquid nitrogen. The reduction schedule consisted of 2 h flowing hydrogen at 393 K, followed by 24 h flowing hydrogen at the desired reduction temperature, which was in the range 643–873 K. After reduction the samples were evacuated to 10^{-4} Pa at 643 K for 2 h to remove chemisorbed hydrogen.

Carbon monoxide chemisorption. CO chemisorption was used to determine the number of surface-exposed metallic iron atoms. The method used was similar to that developed by Emmett and Brunauer (*26, 27*), and used by others (*17, 28*). Accordingly, a CO adsorption isotherm at 193 K (dry ice–acetone) was first obtained on the freshly reduced catalyst. The sample was then warmed to 273 K and evacuated for 1 h at 10^{-3} Pa to remove physisorbed CO. A second isotherm was then obtained at 193 K. The difference between the two isotherms at 13.33 kPa was taken as the amount of chemisorbed CO. Static adsorption measurements were conducted in a conventional greaseless glass high-vacuum adsorption apparatus which was pumped with a mercury diffusion pump backed by a rotary oil pump. Mercury contamination was prevented by a liquid nitrogen trap and a gold wire trap placed between the pump and the manifold. ICP analysis of dissolved samples never detected mercury. Pressures for adsorption measurements were determined with a Texas Instruments Model 145 precision pressure gage. The apparatus has been described in greater detail elsewhere (*29*). Carbon monoxide (99.97%, Linde) was purified by passage through copper turnings held at 473 K, followed by passage through molecular sieves immersed in a dry ice–acetone bath. The helium used for dead-volume measurements (99.995%, Airco) was purified in the same manner, with the molecular sieves immersed in liquid nitrogen.

The number of surface-exposed iron atoms was determined from the amount of chemisorbed CO through the assumption of a 2 : 1 Fe : CO surface stoichiometry (*28*). The surface-average crystallite size was subsequently estimated from the dispersion, D, using the expression (*30*)

$$d_s = \frac{0.9}{D} \tag{1}$$

where, d_s has units of nanometers.

x-Ray diffraction crystallite size. The volume-average size of the iron crystallites, d_v, was determined by x-ray diffraction line-broadening analysis using the Scherrer equation (*31*)

$$d_v = \frac{K_s\lambda}{\beta_{1/2}\cos\theta} \tag{2}$$

where θ and λ are the Bragg angle and wavelength of the radiation, respectively. The value used for the Scherrer constant, K_s, was 0.89. The half-height width of the pure diffraction profile, $\beta_{1/2}$, was obtained from the experimental peak half-height width, $B_{1/2}$, using Warrens correction:

$$\beta_{1/2}^2 = B_{1/2}^2 - b_{1/2}^2. \tag{3}$$

The extent of instrumental broadening, $b_{1/2}$, was determined by scanning iron filings which were annealed at 973 K for 48 h. This treatment ensured large strain-free crystals. The diffractometer was a Philips Model 12215, which utilized Cu$K\alpha$ radiation.

Broadening was measured on the (110) α-iron line at $2\theta = 44.71°$. The peak was scanned at a rate of 0.25° min^{-1}.

Quantitative analysis of support phases. The phase composition of support samples exposed to various conditions was determined by x-ray diffraction analysis. Only anatase and rutile were detected. The anatase–rutile mass ratio, x_A/x_R, was determined by the direct comparison method as described by Cullity (*31*). With this method, the ratio of the integral intensities of a characteristic reflection for each phase, I_A/I_R, is related to the ratio of the mass fractions of each phase by the expression

$$\frac{I_A}{I_R} = \frac{R_A}{R_R}\frac{x_A}{x_R}\frac{\rho_R}{\rho_A} \qquad (4)$$

where ρ_R/ρ_A is the ratio of the density of each phase. The parameter R for each phase is given by the following, which originates from the expression describing the integral intensity of a line in the x-ray diffraction pattern:

$$R = \frac{1}{\nu^2} F^2 p_m \frac{1 + \cos^2 2\theta}{\sin^2 \theta \cos \theta}. \qquad (5)$$

Here, ν is the unit cell volume, F is the structure factor, and p_m is the multiplicity factor. The R values for each phase were evaluated as outlined by Cullity (*31*), and can be found elsewhere (*29*). The intensities were obtained by integrating the peaks in the diffraction patterns using a Gauss–Legendre quadrature (*32*).

Total surface area measurement. The surface area of catalysts exposed to various conditions were measured using the BET method with nitrogen as the adsorbate at liquid nitrogen temperature. Static adsorption measurements were performed in the same adsorption apparatus described above. The nitrogen (Linde, 99.998%) was used with no further purification. For each sample, about 15 points on the isotherm were taken in the p/p_0 range 0.05–0.30. The surface area was obtained from the monolayer uptake using the value of 0.162 nm^2 $molecule^{-1}$ for the cross-sectional area of a nitrogen molecule (*33*).

Sample preparation for transmission electron microscopy. Samples to be examined by transmission electron microscopy were first lightly ground in a mortar and pestle. Five milligrams of the resulting powder was placed in 10 ml of toluene and ultrasonically dispersed for $\frac{1}{2}$ h. A single drop of the suspension was placed on a carbon-coated copper microscope grid, and was allowed to air-dry for 10 min at 340 K. The sample was then placed in the microscope, which was a JEOL 100B instrument. This was similar to the method used by Smith *et al.* (*34*).

RESULTS

Characterization of the Support

Titania samples were exposed to flowing H_2, flowing O_2 (both 1.7 ml s^{-1}), and vacuum (10^{-4} Pa), for 12 h at several temperatures in the range 473–873 K. The BET surface area and phase composition of the samples were subsequently determined. This was done to determine the effect of gaseous environment and temperature on the support morphology and phase composition, over a range of temperatures including the temperature at which SMSI occurs. A sample consisting of 6.8% Fe/TiO_2 was also exposed to flowing H_2, and the support was subsequently characterized to determine the effect of the iron crystallites on the support morphology and phase composition.

The effect of temperature on the BET surface area for titania samples exposed to different atmospheres and for Fe/TiO_2 samples exposed to H_2 is shown in Fig. 1. It is noted that a significant decrease in BET surface area took place for all samples at temperatures in excess of 673 K. Oxygen-treated samples experienced only moderate surface area decrease, while the surface areas of H_2-treated samples were markedly reduced at temperatures between 673 and 873 K. The surface areas of vacuum-treated

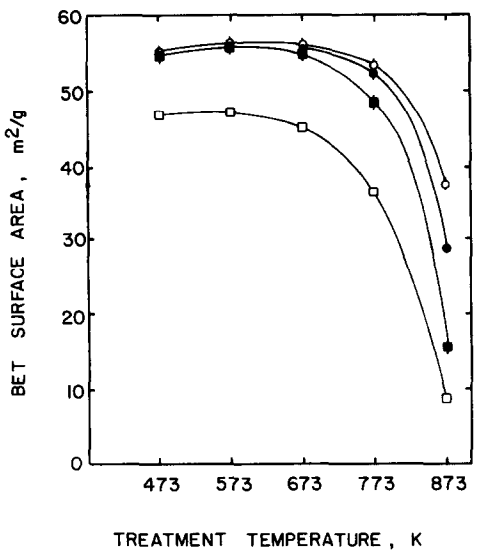

FIG. 1. Effect of temperature and gaseous environment on BET surface area after 12 h exposure: (○) pure TiO_2 in O_2, (■) pure TiO_2 in H_2, (●) pure TiO_2 *in vacuo*, (□) 6.8% Fe/TiO_2 in H_2.

samples were intermediate to those treated with H_2 and O_2. From these results, it is clear that high temperatures and reducing environments accelerate the titania surface area loss. Electron micrographs of samples treated in H_2 at 473 and 873 K indicated that the surface area decrease was due to enlargement of titania grains. The grains of the sample treated at 473 K were about 20–50 nm in diameter, whereas those of the sample treated at 873 K grew to about 50–150 nm in diameter.

Fe/TiO_2 samples treated in the same manner in H_2 experienced drastic surface area reduction between 673 and 873 K. Comparing the data for the blank and iron-loaded titania samples of Fig. 1, it was noted that treatment of pure titania in H_2 at 773 K decreased the surface area by about 13%, while treatment of Fe/TiO_2 under the same conditions caused a 23% loss in surface area. Likewise, treatment of pure TiO_2 at 873 K reduced the surface area by about 72%, while treatment of Fe/TiO_2 under the same conditions reduced the surface area by 81%. Thus, it appears that iron accelerates the surface area decrease and, thus, the grain enlargement process in Fe/TiO_2 samples. The curve for the Fe/TiO_2 samples in Fig. 1 is displaced downward somewhat relative to the curves for the blank support samples. This was due to increased physical contact of the support grains, which was induced during impregnation of the support powder with iron solution. The blank support samples were prepared in a manner similar to the iron-loaded samples, with the exception that distilled water was used instead of iron solution. However, in the preparation of the iron-loaded samples, a significantly higher degree of mixing of the powder with the solution (to ensure uniform loading) produced samples with lower surface area.

The effect of temperature on the anatase percentage for titania samples exposed for 12 h to different atmospheres, and Fe/TiO_2 samples exposed to H_2 for 12 h is presented in Fig. 2. Oxygen-treated samples experienced moderate phase transition at temperatures above 673 K; however, vacuum- and H_2-treated samples experienced more extensive phase transition at temperatures in excess of 673 K. Anatase percentages of

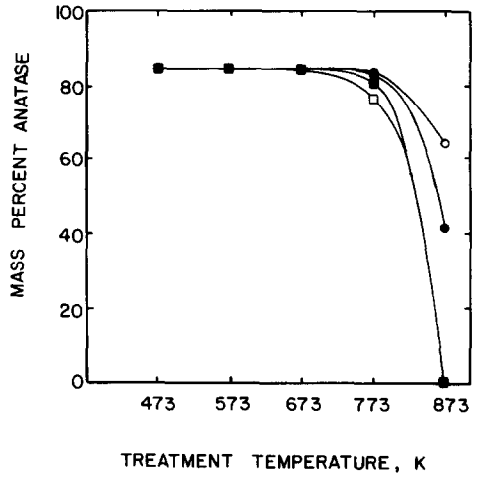

FIG. 2. Effect of temperature and gaseous environment on the support composition after 12 h exposure: (○) pure TiO_2 in O_2, (■) pure TiO_2 in H_2, (●) pure TiO_2 *in vacuo*, (□) 6.8% Fe/TiO_2 in H_2.

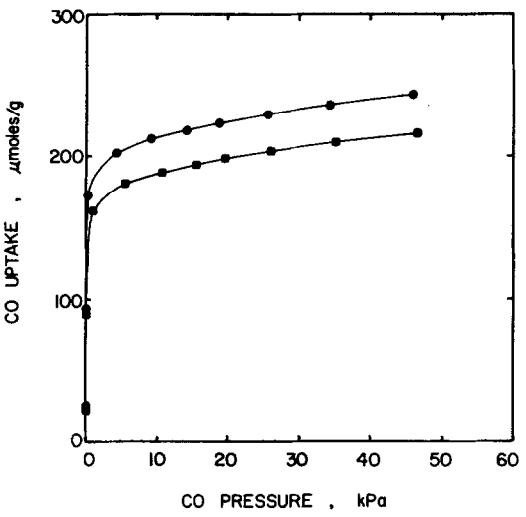

FIG. 3. Carbon monoxide adsorption isotherms for 6.3% Fe/TiO_2 impregnated with saturated $Fe(NO_3)_3 \cdot 9H_2O$ in 1 *M* HNO_3, reduced in hydrogen for 24 h at 643 K: (●) first isotherm, (■) second isotherm.

vacuum-treated samples were intermediate to those of H_2- and O_2-treated samples. For both TiO_2 and Fe/TiO_2 treated in H_2, the phase transition was complete at 873 K. No anatase could be detected in these samples. From these results it is clear that reducing environments and high temperatures accelerate the phase transition. It should be noted that the anatase composition of the Fe/TiO_2 sample after treatment at 773 K is significantly less than that of pure titania treated under the same condition, indicating that the anatase–rutile phase transition is catalyzed by iron.

Characterization of Supported Iron Crystallites

Carbon monoxide chemisorption was used to infer iron particle sizes in various catalyst samples. Adsorption isotherms for a 6.3% Fe/TiO_2 catalyst prepared from $Fe(NO_3)_3 \cdot 9H_2O$ in 1 *M* HNO_3 and reduced at 643 K are shown in Fig. 3. Taking the difference between the two isotherms results in the chemisorption isotherm of Fig. 4. After the first isotherm was obtained, the adsorption cell was warmed to 273 K and evacuated to remove physisorbed CO. This is higher than the temperature usually used with this technique (193 K), since it was determined (*29*) that for the present apparatus, removal of physisorbed CO was too slow at 193 K. Insufficient removal of physisorbed CO results in overprediction of the amount of chemisorbed CO. This was eliminated by warming the sample to 273 K between adsorption isotherms. However, warming the sample introduces the danger of dissociating CO and invalidating the assumed adsorption stoichiometry. The adsorption of CO on polycrystalline iron has been studied by Yu *et al.* (*35*) using ultraviolet photoemission spectroscopy (UPS). They noted that at room temperature both molecular and dissociated forms coexist. In another study, Kishi and Roberts (*36*) showed using UPS that CO adsorption at 80 and 196 K is molecular and stable on polycrystalline iron films. However, at 295 K, CO adsorption was mostly molecular with minor dissociation. This appears to agree with the UPS studies of CO adsorption on (110) iron conducted by Broden *et al.* (*37*), who report only "slow" CO dissociation at 295 K. More recently, Cameron and Dwyer (*38*) have investigated the chemisorption of CO on Fe (100) using XPS, LEED, TPD, and UPS. This study indicated that not only was CO fully associated at temperatures below 300 K, but the surface stoichiometry

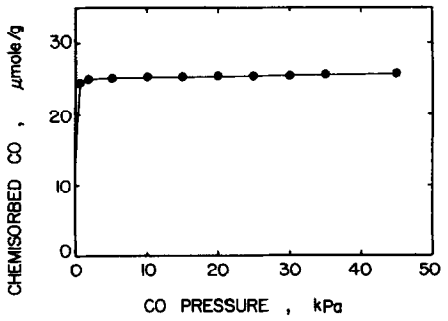

FIG. 4. Carbon monoxide chemisorption isotherm for 6.3% Fe/TiO_2 impregnated with saturated $Fe(NO_3)_3 \cdot 9H_2O$ in 1 *M* HNO_3, reduced in hydrogen for 24 h at 643 K.

TABLE 1

CO Uptake, Dispersion, and Particle Sizes for 6.3% Fe/TiO_2 Prepared with Saturated $Fe(NO_3)_3 \cdot 9H_2O$ in 1 *M* HNO_3 and Reduced in Hydrogen for 24 h at Various Temperatures

Reduction temperature (K)	CO uptake (μmol/g)	Dispersion	d_s (nm)	d_v (nm)	d_v/d_s
643	24.9	0.045	20.0	26.2 ± 1.3	1.31
673	22.7	0.041	22.2	30.1 ± 0.5	1.36
673	23.8	0.043	20.9	—	—
723	14.5	0.026	34.9	41.6 ± 0.9	1.19
773	6.6	0.012	76.9	43.4 ± 1.2	0.56
823	4.1	0.007	123.9	43.8 ± 1.4	0.35
873	1.1	0.002	452.4	37.1 ± 0.9	0.08

is 2 : 1 Fe : CO. In view of these studies, we were not concerned about dissociation of CO after 1 h at 273 K. In a series of experiments it was determined that after evacuation at 273 K for periods of 2 and 3 h, the same result for the amount of strongly held CO was obtained as for the 1-h evacuated samples, suggesting further that CO dissociation at 273 K was not a problem, nor was molecularly chemisorbed CO removed. Furthermore, we have obtained better agreement between x-ray diffraction and CO chemisorption particle sizes than other investigators (*17, 28*) who have kept the sample at 193 K between isotherm measurements. These investigators obtained particle sizes from CO chemisorption that were significantly smaller than those estimated by x-ray diffraction, indicating that CO uptake may have been overpredicted.

Table 1 shows CO chemisorption and x-ray diffraction line-broadening analysis data for several 6.3% Fe/TiO_2 catalysts impregnated with saturated $Fe(NO_3)_3 \cdot 9H_2O$ in 1 *M* HNO_3, and reduced in hydrogen according to the reduction schedule described under Experimental. Fresh samples were reduced at 50 K intervals in the range 643–873 K. The surface-average particle size was calculated from the dispersion using Eq. (1). The volume-average particle size was determined from the Scherrer equation. By performing the same chemisorption measurement for a blank titania sample reduced at 673 K, it was determined that 0.43 μmol CO g^{-1} was chemisorbed to the support. Thus, this quantity was subtracted from the CO uptakes for all iron-loaded samples. Good agreement between particle sizes determined by the two methods is the case for the samples of Table 1 which were reduced in the range 643–723 K. Two identical samples reduced at 673 K verified the reproducibility of the measurement. CO uptakes for catalysts reduced at or above 773 K are increasingly suppressed due to the SMSI effect.

The last column of Table 1 shows the ratio of the volume- and surface-average particle sizes determined by x-ray diffraction and CO chemisorption, respectively. This ratio was found to be a convenient indication of the extent of metal–support interaction. At lower reduction temperatures (643–723 K), the ratio remained fairly constant, not varying by more than about 14%. However, for the catalyst reduced at 773 K, the ratio decreased by more than a factor of 2, and became progressively smaller as the reduction temperature increased. This most likely resulted from blockage of CO adsorption sites by titania adspecies which migrated to the particle surfaces. The slightly smaller particle size ratio at 643 K reduction temperature is probably due to incomplete reduction of iron.

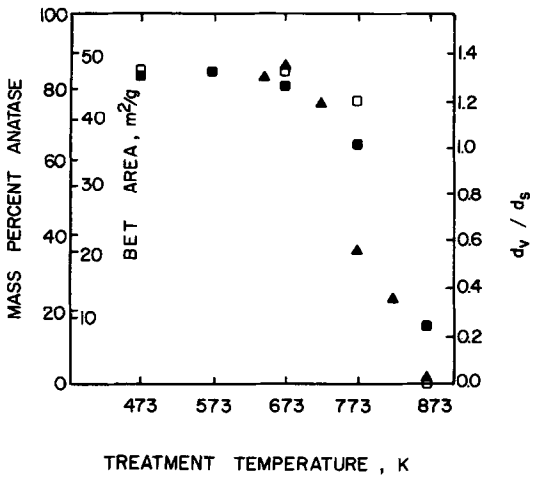

FIG. 5. Plot showing behavior of the various phenomena occurring at the onset of SMSI: (■) BET surface area, (□) mass percentage anatase, (▲) particle size ratio.

Figure 5 shows the particle size ratio of Table 1 plotted against reduction temperature. Also shown on the plot are the BET surface areas and anatase mass percentages for the 6.8% Fe/TiO_2 samples of Figs. 1 and 2, respectively. From Fig. 5 it is evident that anatase–rutile phase transition, enlargement of titania grains, and metal–support interaction appear to have occurred simultaneously, and at increasing extent as the reduction temperature was increased. The onset of these phenomena began at about 723 K.

The crystallite sizes as determined by x-ray diffraction line broadening for 6.3% Fe/TiO_2 samples prepared with the iron salt in 1 *M* HNO_3 (Table 1) are plotted versus reduction temperature in Fig. 6. There are a few features of this plot worth noting. For reduction temperatures in the range 643–723 K, the iron crystallites grew larger as the reduction temperature increased. However, between 723 and 823 K, the particles had less tendency to become larger as the temperature increased, as was evidenced by the decreased slope of the curve in the temperature range 723–823 K. In addition, the temperature at which the slope of the curve significantly decreases corresponds to the temperature in Fig. 5 at which the grain enlargement, phase transition, and SMSI all begin to occur. Another feature worth noting is the unexpected decrease in particle size between 823 and 873 K. The origin of these features is discussed below.

Figure 7 shows a transmission electron micrograph of the 873 K-reduced sample of Table 1. The iron particles appear to have split apart, as evidenced by the existence of pairs of particles shown in the circled regions. In addition, one of the particles appears to have acquired a toroidal shape. This same phenomenon was seen in several other micrographs not shown here.

In an attempt to stabilize the support material, and thereby suppress the SMSI effect, a titania sample was subjected to high-temperature treatment before impregnation with iron. A sample of pure titania was treated in flowing H_2 for 12 h at 873 K. After this treatment, the powder was blue, indicating that it had been reduced (*21*). The sample was then reoxidized in flowing oxygen at 473 K for 4 h, after which it became a light yellow color. x-Ray diffraction confirmed the presence of only rutile. The

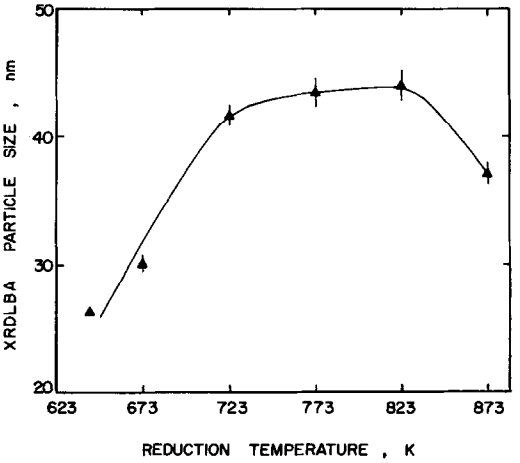

FIG. 6. Particle size determined from X-ray diffraction line-broadening analysis (XRDLBA) for 6.3% Fe/TiO_2 impregnated with saturated $Fe(NO_3)_3 \cdot 9H_2O$ in 1 *M* HNO_3, reduced in hydrogen for 24 h at various temperatures.

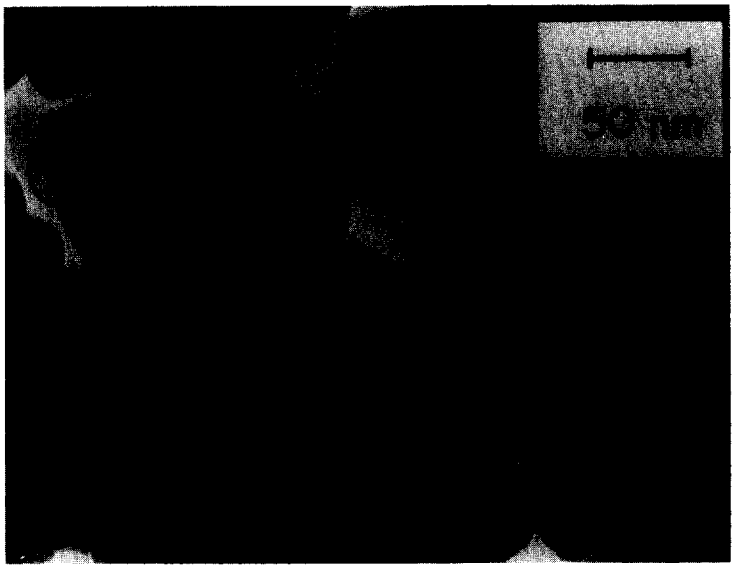

FIG. 7. Transmission electron micrograph of 6.3% Fe/TiO_2 impregnated with saturated $Fe(NO_3)_3 \cdot 9H_2O$ in 1 *M* HNO_3, reduced in hydrogen for 24 h at 873 K.

rutile powder was then impregnated with $Fe(NO_3)_3 \cdot 9H_2O$ in 1 *M* HNO_3, and reduced in a manner identical with the samples of Table 1. Carbon monoxide uptakes, dispersions, and particle sizes for samples reduced at 673 and 773 K are shown in Table 2. The CO uptakes for these samples were much smaller than those of the anatase-supported samples of Table 1 which were reduced at the same temperature. In addition, the particle size ratios for these samples are much smaller than those of Table 1 reduced at the same temperature, indicating poor reduction of iron or drastic interaction with the support. The decrease in the particle size ratio by a factor of 3.1 for the sample reduced at the higher temperature suggests that the metal–support interaction responsible for suppression of CO chemisorption occurred at 773 K. It was also noted that the x-ray diffraction iron particle sizes in the rutile-supported samples were significantly smaller than those of the anatase-supported samples which were reduced at the same temperatures (Table 1).

CO uptakes, dispersions, and particle sizes for catalysts prepared by impregnation with saturated $Fe(NO_3)_3 \cdot 9H_2O$ in 2 *M* HNO_3, and reduced at several tempera-

TABLE 2

CO Uptake, Dispersion, and Particle Sizes for 6.8% Fe/TiO_2 (Rutile) Prepared with Saturated $Fe(NO_3)_3 \cdot 9H_2O$ in 1 *M* HNO_3 and Reduced in Hydrogen for 24 h at Various Temperatures

Reduction temperature (K)	CO uptake (μmol/g)	Dispersion	d_s (nm)	d_v (nm)	d_v/d_s
673	8.7	0.041	64.0	25.6 ± 0.5	0.40
773	2.3	0.004	243.2	30.6 ± 0.8	0.13

TABLE 3

CO Uptake, Dispersion, and Particle Sizes for 6.0% Fe/TiO_2 Prepared with Saturated $Fe(NO_3)_3 \cdot 9H_2O$ in 2 *M* HNO_3 and Reduced in Hydrogen for 24 h at Various Temperatures

Reduction temperature (K)	CO uptake (μmol/g)	Dispersion	d_s (nm)	d_v (nm)	d_v/d_s
643	17.4	0.032	27.9	24.4 ± 0.3	0.87
643	16.4	0.030	29.8	26.7 ± 0.7	0.90
673	22.0	0.041	22.1	31.7 ± 0.9	1.43
773	10.0	0.019	48.4	45.4 ± 2.6	0.94
773[a]	13.1	0.024	37.1	43.7 ± 1.6	1.18

[a] Reduced at 773 K for 24 h, followed by 3-h treatment in O_2, and reduction at 673 K for 24 h.

tures are shown in Table 3. A sample reduced at 643 K exhibited smaller CO uptake and smaller particle size ratio relative to the catalyst prepared with 1 *M* HNO_3 and reduced at the same temperature. This result was verified by reducing a second sample at the same temperature. The particle size ratio for the 673 K-reduced sample is similar to that of the catalysts prepared with 1 *M* HNO_3 (Table 1) and reduced at the same temperature. As was the case with the samples prepared with 1 *M* HNO_3, the catalyst reduced at 773 K exhibited a significantly smaller particle size ratio relative to the 673 K-reduced sample. Another identical sample reduced at 773 K in the same manner, followed by 3 h O_2 treatment (1.7 ml s^{-1}) at 473 K and subsequent reduction in H_2 at 673 K for 24 h, yielded crystallites which were less affected by SMSI. The particle size ratio of 1.18 for this sample is closer to the value obtained for the 673 K-reduced sample, indicating nearly normal behavior of the iron particles. Since the particle size ratio is slightly smaller than that of the 673 K-reduced sample, it appears that the O_2 treatment did not completely restore the particles to a state unaffected by the support.

In an attempt to compare catalysts prepared with aqueous and organic impregnating solvents, a series of samples were prepared by impregnating titania with solutions consisting of saturated $Fe(NO_3)_3 \cdot 9H_2O$ in DMF. The x-ray diffraction and CO chemisorption results for samples reduced at several temperatures are shown in Table 4. As was the case with catalysts prepared with the iron salt dissolved in 2 *M* HNO_3, the ratio of x-ray diffraction and chemisorption particle sizes for the 643 K-reduced sample was significantly smaller than the ratio seen with the catalyst prepared with 1 *M* HNO_3 reduced at 643 K. This is probably due to incomplete iron reduction at the lower temperature. The x-ray diffraction and chemisorption particle sizes for the samples reduced at 673 K are similar to those of the catalysts prepared with the iron salt dissolved in 1 and 2 *M* HNO_3 and reduced at the same temperature. However, at the reduction temperature of 723 K both x-ray diffraction and CO chemisorption indicated smaller particles on the DMF-prepared samples versus the samples prepared using 1 *M* HNO_3.

DISCUSSION

It is well known that titania becomes partially reduced in atmospheres of hydrogen and vacuum. Removal of oxygen from surfaces of anatase and rutile has been inferred by observing sample weight decreases in hydrogen atmospheres (*39*). Reduction is

TABLE 4

CO Uptake, Dispersion, and Particle Sizes for 6.3% Fe/TiO_2 Prepared with Saturated $Fe(NO_3)_3 \cdot 9H_2O$ in Dimethyl Formamide and Reduced in Hydrogen for 24 h at Various Temperatures

Reduction temperature (K)	CO uptake (μmol/g)	Dispersion	d_s (nm)	d_v (nm)	d_v/d_s
643	19.6	0.032	28.6	28.5 ± 0.8	1.00
673	26.2	0.042	21.3	29.2 ± 0.8	1.37
673	25.9	0.042	21.6	26.5 ± 1.2	1.23
723	17.9	0.029	31.2	33.1 ± 1.3	1.06

more severe as the temperature and hydrogen pressure are increased. According to Herrmann and Pichat (*40*), removal of oxygen during reduction results in surface anionic oxygen vacancies by formation of surface hydroxyl groups and subsequent desorption of water. The reduction is represented by the reaction

$$H_2 + 2O^{2-} \rightleftarrows H_2O + O^{2-} + V_{O^{2-}} \quad (6)$$

where $V_{O^{2-}}$ represents a surface anionic vacancy containing two trapped electrons.

More detailed information about the nature of reduced titania has been obtained by ESR spectroscopy. Peaks in the ESR spectra of reduced pure titania (*4–6, 41*) and Pt/TiO_2 (*5*) have been assigned to the presence of Ti^{3+} ions. Gravelle *et al.* (*4*) attributed one peak which was unaffected by oxygen exposure to Ti^{3+} ions in normal lattice or octahedral sites. A second peak, which disappeared after oxygen exposure, was attributed to surface Ti^{3+} ions associated with one or two anionic oxygen vacancies. Cornaz *et al.* (*6*) also observed peaks in the ESR spectra of reduced titania which remained when samples were exposed to oxygen, but attributed these to bulk Ti^{3+} ions. Other work has indicated that surface Ti^{3+} ions can migrate into the bulk lattice during reduction (*41*).

Above it was noted that enlargement of titania grains and the anatase–rutile phase transition were accelerated under reducing conditions. During phase transition, the elongated anatase crystal form rearranges to the shorter rutile form. This process involves a rearrangement of the majority of the Ti^{4+} ions by rupture of two of the six Ti–O bonds in the unit cell to form new bonds (*42, 43*). Under reducing conditions, as described above, anionic vacancies and/or Ti^{3+} ions are present on the surface and in the bulk. It is likely that rupture of a Ti–O bond would be more favorable under these conditions, since a titanium cation produced by bond rupture would be stabilized by the excess negative charge in the lattice. Thus, the presence of Ti^{3+} defect centers could provide sites at which nucleation of the rutile phase occurs. The rupture of these bonds and the simultaneous phase transition result in a highly chaotic state where rapid diffusion is occurring. The higher rates of titania grain growth under reducing conditions observed above indicates that diffusion of the support material is more rapid in reducing environments.

It was also noted in Fig. 5 that the support grain enlargement, the anatase-rutile phase transition, and the SMSI occurred simultaneously and at increasing extents as the reduction temperature was increased above 723 K. Simultaneous occurrence of these three phenomena suggests that they are interrelated, and that grain enlargement and phase transition are important factors concerning SMSI in high-surface-area titania-supported catalysts. From these observations, the following picture seems to

emerge. At reduction temperatures in hydrogen of 723 K and higher, the support becomes significantly reduced. Ti^{3+} ions and anionic vacancies are present on the surface and in the bulk. Support reduction is enhanced by the presence of reduced iron crystallites and their ability to dissociate hydrogen (*5, 44, 45*). The increased concentration of Ti^{3+} ions causes an increase in the rate of rupture of Ti–O bonds in the lattice and near the surface. This higher rate of Ti–O bond rupture facilitates large-scale rearrangement of the lattice as the phase transition takes place. Thus, during phase transition, a chaotic condition exists, where rapid migration of titanium–oxygen species, titanium ions, and oxygen ions is occurring. These migrating species encounter the reduced iron particles, and are stabilized by reaction with them to form a mixed surface oxide:

$$Fe + TiO_x \rightarrow FeTiO_x. \qquad (7)$$

This renders the iron no longer capable of chemisorbing CO.

The characterization data presented in Table 2 indicate that the SMSI phenomenon also occurs with rutile-supported metals reduced at 773 K. Thus, it cannot be concluded that phase transition is entirely responsible for the occurrence of SMSI in anatase samples. Rather, it is likely that the phase transition plays an important role in the SMSI mechanism in anatase samples. It was recently shown by Lane and Wolf (*46*) that SMSI is more pronounced on anatase-supported Pt versus rutile-supported Pt. In addition, these authors suggest that the site blockage mechanism is different for the rutile catalysts. This is likely due to the phase transition occurring during reduction of the supported metal. Kikuchi *et al.* (*47*) investigated the CO hydrogenation reaction over Ru supported on both crystal forms of titania. They observed higher activities and a larger fraction of higher-molecular-weight hydrocarbons over the rutile-supported catalysts. Hydrogen chemisorption measurements by these investigators for Ru supported on both crystal forms reduced at 723 K indicated higher H_2 uptakes for the rutile catalysts. This indicates that SMSI may have been more pronounced on the anatase-supported samples, suggesting that the anatase–rutile phase transition may play a role in the SMSI effect. Determination of the exact manner in which the anatase–rutile phase transition influences the SMSI properties of supported metals would require further study.

From Fig. 6 it was observed that the x-ray diffraction particle size increased with temperature for reduction temperatures between 643 and 723 K. However, between 723 and 823 K the particles had less tendency to grow as the reduction temperature was increased. It was also noted that a decrease in particle size took place as the reduction temperature was increased from 823 to 873 K. The initially strong dependence of particle size on temperature in the range 643–723 K would at first appear to be the result of normal sintering of iron particles. However, when considering the details of iron reduction on oxide supports, another process may be occurring in this temperature range. When Fe^{3+} ions are reduced in hydrogen, metallic iron particles are formed from reduction of Fe^{3+} ions which migrate over the support surface. Once large metallic iron particles are formed due to this migration, this seems to accelerate the full reduction of iron (*48*). For weak metal–support interaction, iron can be reduced to large metallic particles. However, for strong metal–support interaction, reduction of iron ions is difficult due to their inability to migrate over the support and combine to form large particles. This is the case with iron supported on alumina, where it is believed that Fe^{2+} ions are stabilized by occupation of empty octahedral sites on the alumina surface (*49*). This is thought to be the reason that iron is incompletely reduced on alumina even at high reduction temperatures. For iron supported on titania, Tau and Bennett (*21*) determined the percentage of zero-valent iron for 10%

Fe/TiO_2 catalysts using Mössbauer spectroscopy. They determined that for 24-h reduction in hydrogen at 723 K, 91.2% of the iron was in the zero-valent state, and at 773 K, iron was completely reduced. Thus, in the present study, at lower temperatures (643–723 K) iron particles probably grow by migration of ferric ions over the support surface, since reduction of iron is not complete. Once the particles become fully reduced (723–773 K) the mechanism of particle growth would likely change, and thus a change in the rate of particle growth is possible. Thus, the decreased tendency of iron particles to become larger with increasing reduction temperature between 723 and 823 K may represent a change in the mechanism of particle growth.

It has been shown in previous investigations that particles supported on titania are stabilized against high-temperature sintering when in the SMSI state (*12, 25, 50, 51*). The particle stabilization phenomenon at temperatures between 723 and 823 K, noted in Fig. 6, might be due to this effect. It is believed that this is the most likely reason for the observed stabilization of particle growth. This is supported by the fact that the temperature at which the slope of the curve in Fig. 6 significantly changes (~723 K) coincides with the temperature in Fig. 5 at which BET surface area, anatase–rutile phase transition, and ratio of x-ray and chemisorption particle sizes begin to show significant decreases (onset of SMSI).

The x-ray diffraction particle size in Fig. 6 sharply decreased as the reduction temperature was increased from 823 to 873 K. This result may be explained by the micrograph (Fig. 7), which indicated that the particles fractured and formed toroids. Splitting of iron particles, and toroid formation has also been observed in Fe/Al_2O_3 (*52*) and Fe/TiO_2 (*53*) model catalysts. This would explain the decrease in x-ray diffraction particle size. It has also been suggested that at high temperatures, the metal may begin to diffuse into the titania support (*10, 11*). This might also cause broadening of the x-ray lines. Tatarchuk and Dumesic (*11*) with a model Fe/TiO_2 catalyst have observed diffuse spreading of the particles and diffusion into the support at 873 K. Indeed, spreading and thinning of particles would cause broadening of the x-ray lines.

Table 2 presented CO chemisorption and x-ray diffraction results for samples supported on rutile which were reduced at 673 and 773 K. Since only small amounts of CO were taken up by these samples after reduction at 673 K, it appears that the extent of iron reduction was small. x-Ray diffraction indicated particles significantly smaller than those of the anatase-supported samples reduced at the same temperature. To explain these results, consideration must be given to the manner in which the support was treated before impregnation. The titania powder was first reduced in hydrogen to induce the anatase–rutile phase transition. It was then reoxidized with oxygen at 473 K and subsequently impregnated with iron and reduced in the normal manner. ESR measurements by other investigators have indicated that when reduced titania is treated with oxygen, O_2^- ions become adsorbed to anionic vacancies (*4, 6*). Cornaz *et al.* (*6*) showed that when oxygen-deficient TiO_2 is subjected to O_2 at room temperature, several forms of surface oxygen complexes are formed. The bonding between oxygen and surface titanium cations is similar to metal–ligand bonds in transition metal complexes. These adsorbed oxygen anions may have reacted with Fe^{2+} and/or Fe^{3+} ions during support reduction, resulting in surface complexes of the form Ti–O–Fe or Ti–O–O–Fe. This would prevent migration of unreduced iron over the support during reduction and would inhibit the formation of large reduced iron particles. This would have the same effect as the stabilization of Fe^{2+} ions by occupation of octahedral sites on alumina surfaces.

The ratio of x-ray diffraction and chemisorption particle sizes for the 773 K-reduced rutile-supported iron sample was smaller than that of the 673 K-reduced sam-

ple by a factor of about 3.1, suggesting that SMSI still took place. Thus, thermal stabilization of the support apparently does not inhibit metal–support interaction.

Above it was shown (Table 3) that oxidation of catalysts in the SMSI state and subsequent low-temperature reduction render the supported particles back to a nearly normal state. This phenomenon has also been reported by others (*7, 13, 17*). This type of result is difficult to rationalize in terms of the migration of a reduced titania species to the metal particle surface. The migrating species is evidently in a highly reactive form which is stabilized by reaction with the reduced metal, preventing chemisorption of H_2 or CO. In the SMSI state, the titania species is probably present as a near-monolayer film covering the particles. Oxidation and subsequent reduction at 673 K cause a modification of the metal particle surface such that clean iron surfaces are exposed after reduction, allowing CO chemisorption. The following mechanism is proposed to explain this. When the SMSI-affected surface is oxidized, the oxides of each metal are formed according to the following reaction:

$$FeTiO_x + (7 - 2x)O_2 \rightarrow \tfrac{1}{2}Fe_2O_3 + TiO_2. \quad (8)$$

Titanium dioxide formed during this oxidation would no longer be spread over the iron surface, but would probably sinter and form small titania crystallites on the iron particle surface. During reduction at 673 K, iron oxide would be reduced to metallic iron, and further sintering of titania would occur, but the small titania particles would not be reduced, and thus would not interact strongly with iron. The small titania aggregates would cause some blockage of reduced metal sites, but would be much less efficient in covering the particle surfaces than the migrating titania species formed during reduction at 773 K. This also explains why oxidation followed by low-temperature reduction does not fully restore normal behavior in most reported cases.

The ratios of x-ray diffraction and CO chemisorption particle sizes determined for catalysts impregnated with the iron salt in 2 *M* HNO_3 and DMF (Tables 3 and 4, respectively), which were reduced at 643 K, were smaller than those of samples reduced at 673 K. As the reduction temperature was increased from 643 to 673 K, most likely, further reduction of iron caused an increase in the particle size ratio due to higher CO uptake. For the catalysts prepared with 1 *M* HNO_3 (Table 1), the particle size ratio for the catalyst reduced at 643 K was about the same as that of the sample reduced at 673 K. Thus, for the samples prepared using 2 *M* HNO_3 and DMF impregnating solvents, iron was apparently not as easily reduced as with the samples prepared using 1 *M* HNO_3. The acid concentration of aqueous iron impregnating solutions has been shown to have an effect on the extent of iron reduction with other oxide supports (*54*). Apparently, this is related to the hydrolysis of iron in aqueous solution. In solution, iron undergoes hydrolysis with water. The hydrolyzed form subsequently dimerizes via formation of linear Fe–O–Fe bonds (*55*). Large multinuclear structures are subsequently formed in solution by combination of these dimers. Higher acid concentration suppresses hydrolysis and formation of these structures. During impregnation, these multinuclear complexes are deposited on the surface of the support. If these are present, metallic iron particles might be more easily formed at lower reduction temperatures due to the close proximity of ferric ions in the deposited complexes. At lower acid concentration, a greater extent of formation of these multinuclear iron complexes is expected. This may be the reason for the higher extent of iron reduction at 643 K with the catalyst prepared from $Fe(NO_3)_3 \cdot 9H_2O$ in 1 *M* HNO_3 (as suggested by the higher particle size ratio). The lower water concentration in the DMF impregnating solution may have resulted in a smaller extent of iron hydrolysis, and may be the reason for the low extent of iron re-

duction at 643 K (smaller particle size ratio) as compared with 1 *M* HNO_3 sample.

CONCLUSIONS

It was determined that the onset of the SMSI state in powdered titania samples containing mostly anatase appears to involve a complex scheme where anatase–rutile phase transition, titania grain enlargement, and SMSI occur simultaneously at reduction temperatures higher than 723 K. It was proposed that these phenomena are interrelated, and that Ti^{3+} ions from support reduction initiate the phase transition and grain enlargement, and that the diffusing TiO_x species which migrates to particle surfaces is produced during the chaotic state of phase transition and grain enlargement. The fact that the SMSI phenomenon also occurs in rutile samples indicates that the anatase–rutile phase transition is not entirely responsible for SMSI. However, SMSI may be an important factor with anatase-supported metals. In the temperature range 723–823 K, iron particles were relatively stabilized against high-temperature sintering. The temperature at which this effect was first noted corresponds closely with the temperature of the onset of SMSI, indicating that SMSI was responsible for the stabilization against high-temperature sintering. At the reduction temperature of 873 K, iron particles appeared to split and form toroids, and/or the metal may be diffusing into the support. Iron particles supported on rutile were significantly smaller than those supported on anatase which were reduced at the same temperature. In addition, the extent of iron reduction appeared to be less on the rutile samples. The difference was attributed to O_2^- anions adsorbed to titania, which resulted from reduction and subsequent oxidation to induce the anatase–rutile phase transition. These adsorbed O_2^- ions apparently acted to anchor Fe^{3+} and/or Fe^{2+} ions to the support, preventing their migration and combination with reduced iron particles.

ACKNOWLEDGMENT

One of the authors (A.N.) thanks the Carolina Eastman company for a graduate research fellowship.

REFERENCES

1. Tauster, S. J., Fung, S. C., and Garten, R. L., *J. Amer. Chem. Soc.* **100,** 170 (1978).
2. Tauster, S. J., and Fung, S. C., *J. Catal.* **55,** 29 (1978).
3. Horsley, J. A., *J. Amer. Chem. Soc.* **101,** 2870 (1979).
4. Gravelle, P. C., Juillet, F., Meriaudeau, P., and Teichner, S. J., *Disc. Faraday Soc.* **52,** 140 (1971).
5. Huizinga, T., and Prins, R. J., *J. Phys. Chem.* **85,** 2156 (1981).
6. Cornaz, P. F., van Hooff, J. H. C., Pluijm, F. J., and Schuit, G. C. A., *Disc. Faraday Soc.* **41,** 290 (1966).
7. Meriaudeau, P., Ellestad, O. H., Dufaux, M., and Naccache, C., *J. Catal.* **75,** 243 (1982).
8. Sexton, B. A., Hughes, A. E., and Foger, K., *J. Catal.* **77,** 85 (1982).
9. Chien, S. H., Shelimov, B. N., Resasco, D. E., Lee, E. H., and Haller, G. L., *J. Catal.* **77,** 301 (1982).
10. Kao, C. C., Tsai, S. C., Bahl, M. K., Chung, Y. W., and Lo, W. J., *Surf. Sci.* **95,** 1 (1980).
11. Tatarchuk, B. J., and Dumesic, J. A., *J. Catal.* **70,** 335 (1981).
12. Baker, R. T. K., Prestridge, E. B., and Garten, R. L., *J. Catal.* **56,** 390 (1979).
13. Baker, R. T. K., Prestridge, E. B., and Garten, R. L., *J. Catal.* **59,** 293 (1979).
14. Simoens, A. J., Baker, R. T. K., Dwyer, D. J., Lund, C. R. F., and Madon, R. J., *J. Catal.* **86,** 359 (1984).
15. Sadeghi, H. R., and Henrich, V. E., *J. Catal.* **87,** 279 (1984).
16. Spencer, M. S., *J. Catal.* **93,** 216 (1985).
17. Santos, J., Phillips, J., and Dumesic, J. A., *J. Catal.* **81,** 147 (1983).
18. Resasco, D. E., and Haller, G. L., *J. Catal.* **82,** 279 (1983).
19. Jiang, X. Z., Hayden, T. F., and Dumesic, J. A., *J. Catal.* **83,** 168 (1983).
20. Raupp, G. B., and Dumesic, J. A., *J. Catal.* **97,** 85 (1986).
21. Tau, L. M., and Bennett, C. O., *J. Catal.* **89,** 285 (1984).
22. Rao, C. N. R., *Canad. J. Chem.* **39,** 498 (1961).
23. Cimino, A., Gazzoli, D., and Valigi, M., *J. Less-Common Met.* **75,** 85 (1980).
24. El-Akkad, T. M., *J. Colloid Interface Sci.* **76,** 67 (1980).
25. Shastri, A. G., Datye, A. K., and Schwank, J., *J. Catal.* **87,** 265 (1984).
26. Brunauer, S., and Emmett, P. H., *J. Amer. Chem. Soc.* **57,** 1754 (1935).

27. Emmett, P. H., and Brunauer, S., *J. Amer. Chem. Soc.* **59,** 1553 (1937).
28. Boudart, M., Delbouile, A., Dumesic, J. A., Khammonma, S., and Topsøe, H., *J. Catal.* **37,** 486 (1975).
29. Nobile, A., Ph.D. dissertation, University of South Carolina, 1986.
30. Boudart, M., and Djega-Mariadassou, G., "Kinetics of Heterogeneous Catalytic Reactions." Princeton Univ. Press, Princeton, NJ, 1984.
31. Cullity, B. D., "Elements of X-Ray Diffraction." Addison–Wesley, Menlo Park, CA, 1956.
32. Carnahan, B., Luther, H. A., and Wilkes, J. O., "Applied Numerical Methods." Wiley, New York, 1969.
33. Anderson, J. R., "Structure of Metallic Catalysts." Academic Press, New York, 1975.
34. Smith, J. S., Thrower, R. A., and Vannice, M. A., *J. Catal.* **68,** 270 (1981).
35. Yu, K. Y., Spicer, W. E., Lindau, I., Pianetta, P., and Lin, S. F., *Surf. Sci.* **57,** 157 (1976).
36. Kishi, K., and Roberts, M. W., *J. Chem. Soc. Faraday Trans. 1* **71,** 1715 (1975).
37. Broden, G., Gafner, G., and Bonzel, *Appl. Phys.* **13,** 333 (1977).
38. Cameron, S. D., and Dwyer, D. J., *Langmuir* **4,** 282 (1988).
39. Iwaki, T., Komuro, M., Hirosawa, K., and Miura, M., *J. Catal.* **39,** 324 (1975).
40. Herrmann, J., and Pichat, P., *J. Catal.* **78,** 425 (1982).
41. Iyengar, R. D., Codell, M., Gisser, H., and Weisberg, J., *Z. Phys. Chem. NF* **89,** (Suppl.), 325 (1974).
42. Shannon, R. D., and Pask, J. A., *J. Amer. Ceram. Soc.* **48,** No. 8 (1968).
43. Shannon, R. D., *J. Appl. Phys.* **35**(11), 3414 (1964).
44. Kock, A. J. H. M., and Geus, J. W., *Prog. Surf. Sci.* **20,** No. 3 (1985).
45. Baker, R. T. K., Prestridge, E. B., and Murrell, L. L., *J. Catal.* **79,** 348 (1982).
46. Lane, G. S., and Wolf, E. E., *J. Catal.* **105,** 386 (1987).
47. Kikuchi, E., Nomura, H., Matsumoto, M., and Morita, Y., *Pan-Pac. Synfuels Conf.* **1,** 216 (1982).
48. Guczi, G., *Catal. Rev. Sci. Eng.* **23,** 329 (1981).
49. Garten, R. L., and Ollis, D. F., *J. Catal.* **35,** 232 (1974).
50. Seyedmonir, S. R., Strohmayer, D. E., Guskey, G. J., Geoffroy, G. L., and Vannice, M. A., *J. Catal.* **93,** 288 (1985).
51. Foger, K., *J. Catal.* **78,** 406 (1983).
52. Sushumna, I., and Ruckenstein, E., *J. Catal.* **94,** 239 (1985).
53. Tatarchuk, B. J., Chludzinski, J. J., Sherwood, R. D., Dumesic, J. A., and Baker, R. T. K., *J. Catal.* **70,** 433 (1981).
54. Guczi, L., Matusek, K., and Eszterle, M., *J. Catal.* **60,** 121 (1979).
55. Cotton, F. A., and Wilkinson, G., "Advanced Inorganic Chemistry." Wiley, New York, 1980.